JOURNAL OF GEOPHYSICAL RESEARCH, VOL. 112, D10S21, doi:10.1029/2006JD007736, 2007

Nanoparticle growth following photochemical α- and β-pinene oxidation at Appledore Island during International Consortium for Research on Transport and Transformation/Chemistry of Halogens at the Isles of Shoals 2004

L. M. Russell,[1] A. A. Mensah,[1,2] E. V. Fischer,[3,4] B. C. Sive,[5] R. K. Varner,[5] W. C. Keene,[6] J. Stutz,[7] and A. A. P. Pszenny[3,5]

Received 30 June 2006; revised 8 March 2007; accepted 4 April 2007; published 19 May 2007.

[1] Nanoparticle events were observed 48 times in particle size distributions at Appledore Island during the International Consortium for Atmospheric Research on Transport and Transformation/Chemistry of Halogens on the Isles of Shoals (ICARTT/CHAiOS) field campaign from 2 July to 12 August of 2004. Eighteen of the nanoparticle events showed particle growth and occurred during mornings when peaks in mixing ratios of α- and β-pinene and ozone made production of condensable products from photochemical oxidation probable. Many pollutants and other potential precursors for aerosol formation were also at elevated mixing ratios during these events, including NO, HNO_3, NH_3, HCl, propane, and several other volatile organic carbon compounds. There were no consistent changes in particle composition, although both submicron and supermicron particles included high maximum concentrations of methane sulfonate, sulfate, iodide, nitrate, and ammonium during these events. Nanoparticle growth continued over several hours with a nearly linear rate of increase of diameter with time. The observed nanoparticle growth rates varied from 3 to 13 nm h^{-1}. Apparent nanoparticle aerosol mass fractions (yields) were estimated to range from less than 0.0005 to almost 1 using α- and β-pinene as the presumed particle source. These apparent high aerosol mass fractions (yields) at low changes in aerosol mass are up to two orders of magnitude greater than predictions from extrapolated laboratory parameterizations and may provide a more accurate assessment of secondary organic aerosol formation for estimating the growth of nanoparticles in global models.

Citation: Russell, L. M., A. A. Mensah, E. V. Fischer, B. C. Sive, R. K. Varner, W. C. Keene, J. Stutz, and A. A. P. Pszenny (2007), Nanoparticle growth following photochemical α- and β-pinene oxidation at Appledore Island during International Consortium for Research on Transport and Transformation/Chemistry of Halogens at the Isles of Shoals 2004, *J. Geophys. Res.*, *112*, D10S21, doi:10.1029/2006JD007736.

1. Introduction

[2] Atmospheric sources of new particles from gas phase precursors are of significant interest for climate because of their potential to grow into additional new particles that are large enough to act as cloud condensation nuclei (CCN) or to provide additional particles with high surface area to volume for heterogeneous reactions. Gas-to-nanoparticle conversion differs from gas-to-large-particle processes because it increases the number of CCN-sized particles, with these ~100 nm particles also having longer lifetimes than nanoparticles. This in situ production of new, CCN-sized particles comes only from those particles that are nucleated by homogeneous, ion-induced, or other nucleation processes and then grow large enough before coagulating or being lost by other removal processes to act as CCN. For this reason, the gas phase constituents that control the growth of recently nucleated particles that are smaller than 20 nm to particles over 90 nm in size is the central question of this study.

[3] A comprehensive review by *Kulmala et al.* [2004] provides important context for similar measurements of

[1]Scripps Institution of Oceanography, University of California, San Diego, La Jolla, California, USA.
[2]Also at Department of Chemistry, University of Cologne, Cologne, Germany.
[3]Mount Washington Observatory, University of New Hampshire, Durham, New Hampshire, USA.
[4]Now at Department of Atmospheric Sciences, University of Washington, Seattle, Washington, USA.
[5]Climate Change Research Center, Institute for the Study of Earth, Oceans, and Space, University of New Hampshire, Durham, New Hampshire, USA.
[6]Department of Environmental Science, University of Virginia, Charlottesville, Virginia, USA.
[7]Department of Atmospheric and Ocean Sciences, University of California, Los Angeles, California, USA.

0148-0227/07/2006JD007736$09.00

nanoparticle growth at sites spanning many regions and source types. An observational campaign at Appledore Island, Maine, provided a good opportunity for sampling a variety of different sources and precursors, which are typical of the U.S. east coast [*Fischer et al.*, 2006]. The novel aspect of this site for studying new particle formation is that many different precursors that may contribute to growth of nanoparticles are present when air masses arrive from very different source regions. The site is located approximately 10 km offshore of Portsmouth, New Hampshire, and is frequently impacted by urban emissions from Boston and other more distant industrialized cities on the U.S. east coast, with associated high concentrations of O_3, NO_x, and SO_2. Previous work in the region has shown that regional transport greatly affects the day-to-day chemical composition of the boundary layer [*Jordan et al.*, 2000; *Mao and Talbot*, 2004]. Along the nearby coast local sources include emissions from evergreen and deciduous forests and agricultural activities [*Griffin et al.*, 2004], from which biogenic VOCs, including α- and β-pinene and isoprene, are present at high mixing ratios. In addition, the composition of air measured at Appledore Island is influenced by NH_3 emissions over the continent, particularly from agricultural activities [*Smith et al.*, 2007], and by emissions of halogen and sulfur compounds from marine and coastal sources [*Zhou et al.*, 2005]. All of these precursors could effectively provide a gas phase source for nanoparticle growth [*Kulmala et al.*, 2004; *Stanier et al.*, 2004].

[4] Which of these potential precursors are actually responsible for growth will vary with the air mass trajectories and regional sources that determine the mixture of pollutants that occur during individual days. Because of the varied nature of the atmospheric chemical composition at Appledore Island, this study provides a good opportunity to evaluate the conditions under which nanoparticle growth events frequently occur. During this measurement campaign, growth of small particles from below 20 to above 90 nm was observed most frequently directly following diurnal peaks in α- and β-pinene mixing ratios, associated with emissions from local forests. While there were more than five different types of nanoparticle events identified, more than one third of all of the nanoparticle events and more than three quarters of the events in which nanoparticle growth was observed are closely linked to α- and β-pinene emissions.

[5] A number of ground-based field studies have observed nanoparticle formation or growth associated with emissions from forests. One popular site for a number of nanoparticle studies is the boreal forest region of southern Finland, where continuous observations from 1996 have characterized the statistical trends and seasonal patterns of nanoparticles [*Mäkelä et al.*, 1997, 2000a, 2000b; *Aalto et al.*, 2001; *Janson et al.*, 2001; *Kulmala et al.*, 2001, 2004; *Dal Maso et al.*, 2002]. Nanoparticle growth was observed in eucalyptus forests in Portugal [*Kavouras et al.*, 1998, 1999], pine forests in the northern Sierras [*Lunden et al.*, 2006], and pine forests in rural and mountainous parts of Germany [*Birmili et al.*, 2000, 2003; *Held et al.*, 2004]. Perhaps the study with the closest proximity to the Appledore Island site was at Nova Scotia, where α- and β-pinene-related nanoparticle growth was estimated to occur with a yield of 13% [*Leaitch et al.*, 1999]. A comparative overview of these studies along with many other types of both continental and marine observations of nanoparticle growth is presented by *Kulmala et al.* [2004].

[6] Smog chamber experiments have shown that secondary oxidation products of α- and β-pinene contribute to the formation of nanoparticles and their further growth [*Hatakeyama et al.*, 1989]. Various products have been detected in field and laboratory studies [*Atkinson and Arey*, 2003; *Bilde and Pandis*, 2001; *Zhang et al.*, 2004], wherein carboxylic acids (including pinonic acid) and dicarboxylic acids (including pinic acid) are the most prominent secondary products in ozone oxidation of α- and β-pinene. Recent studies [*Kalberer et al.*, 2004] point toward a polymerization of intermediate compounds resulting in polymers or toward sulfate esterification of isoprene oxidation products resulting in organosulfate compounds [*Gao et al.*, 2006].

2. Measurements and Methods

[7] Aerosol sampling on Appledore Island, Maine, during 2004 for the International Consortium for Atmospheric Research on Transport and Transformation/Chemistry of Halogens on the Isles of Shoals (ICARTT/CHAiOS) field campaign began 2 July and continued until 12 August. Particle and gas phase measurements included a broad range of in situ and remote, online and offline chemical instruments [*Fehsenfeld et al.*, 2006]. Local temperatures at ground level varied between 13 and 26°C with generally high relative humidity and frequent fog and rain. There were 19 distinct precipitation events ranging from a

Figure 1. (a–f) Particle size distributions and gas phase precursors measured at Appledore Island during ICARTT/CHAiOS 2004 with air mass classifications. The *x* axis for all plots provides the day and month of the year with ticks marking midnight in local (Eastern) daylight time (EDT). The bottom part of each plot provides a contour plot of the particle size distributions, reported as $dN/dlogD_p$ concentrations [cm^{-3}] given in the color bar in the bottom right of Figure 1f, and mobility diameter [nm] given on the *y* axis. The approximate start and stop times of the 18 nanoparticle events in the category of "growth with α- and β-pinene" are indicated with dashed vertical lines as guides for the eye and numbered at the top by the event number. For 12 of these growth events, modal mean diameters were fit to the nanoparticle mode and are indicated by black plus signs, and the fit to the growth is shown as a white line. The middle part of each plot indicates the air mass classifications with northwesterly (NW) in yellow, midwest (MW) in orange, southwest (SW) urban in red, south coastal in purple, marine in blue, and northern New England (NNE) and eastern (E) Canada in green. The top part of each plot shows the mixing ratios of α-pinene [pptv] as red (lines), β-pinene [pptv] as green (crosses), isoprene [pptv] as blue (ticks), and O_3 [2 × ppbv] as purple (pluses). O_3 is shown from DOAS when it was available, and AIRMAP O_3 was substituted for 2 to 9 July.

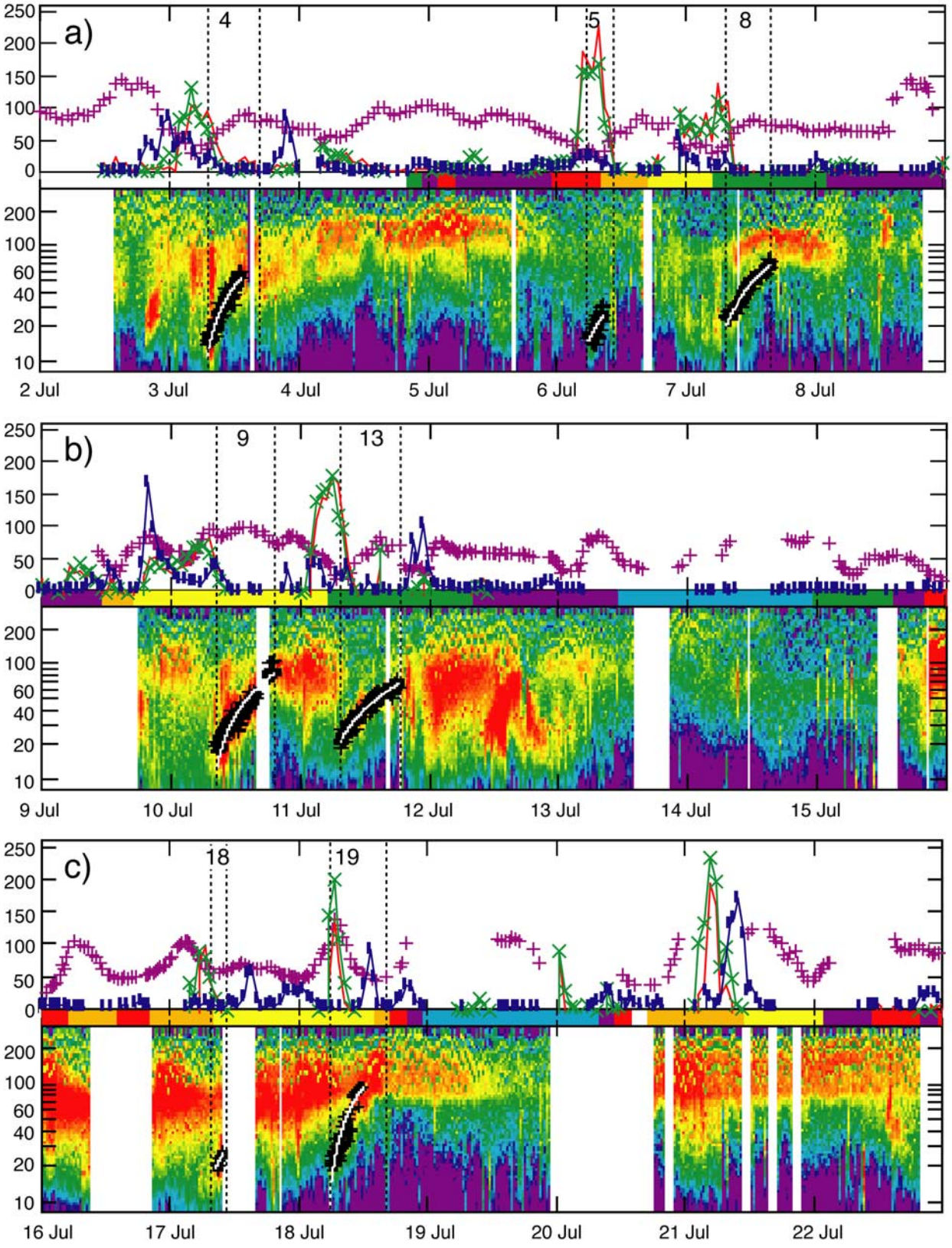
a)
4
5
8
250
200
150
100
50
0
200
100
60
40
20
10
2 Jul
3 Jul
4 Jul
5 Jul
6 Jul
7 Jul
8 Jul
b)
9
13
9 Jul
10 Jul
11 Jul
12 Jul
13 Jul
14 Jul
15 Jul
c)
18
19
16 Jul
17 Jul
18 Jul
19 Jul
20 Jul
21 Jul
22 Jul

Figure 1

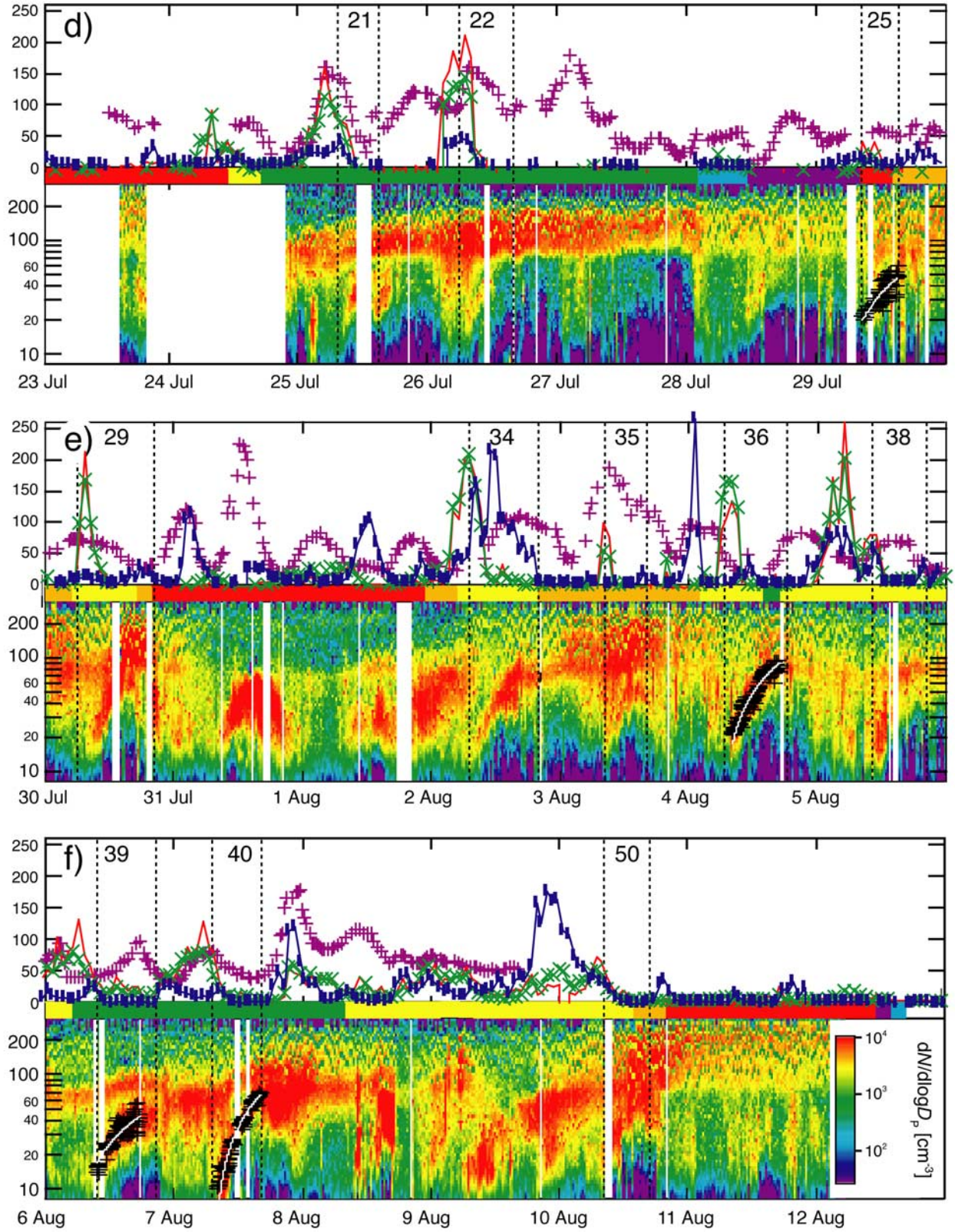

Figure 1. (continued)

sprinkling to 11 mm of rain. Of these, only two events were significant, with rainfall amount greater than 1 mm of rain and duration longer than 1 hour. There were nine fog episodes, defined as periods where the ambient temperature at the surface was equal to the dew point. These events ranged from a few hours to several days in length.

[8] Regional-scale atmospheric transport was evaluated using both HYbrid Single-Particle Lagrangian Integrated Trajectory (HYSPLIT) back trajectories [*Draxler and Rolph*, 2005] and Lagrangian particle dispersion (FLEXPART) retroplumes [*Stohl et al.*, 2003, 2005; *Seibert and Frank*, 2004]. Transport to Appledore Island during the ICARTT study was categorized into six regional flow sectors based on the locations of the 3-day back trajectories [*Fischer et al.*, 2006]. These regional sectors are indicated by color bars along the middle of each part of the timeline in Figure 1. The models used are adequate to classify regional-scale air mass motions impacting Appledore Island during ICARTT/CHAiOS 2004, but they do not account for smaller-scale local transport such as the sea breeze.

2.1. Aerosol Number Size Distributions

[9] Aerosol physical measurements were located on the roof at the top of the observation tower on Appledore Island at 43 m asl (further details are provided by *Fischer et al.* [2006]). The measurements were housed in a ruggedized shipping box fitted with a short vertical inlet with a rain hat, followed by a sharp cut cyclone (BGI model 2.229, http://www.bgiusa.com) with a 1 μm cut-point and diffusion dryer. Submicron particle number distributions were measured by a scanning-type differential mobility analyzer (DMA) that used a TSI 3071 Electrostatic Classifier and a TSI 3010 Condensation Particle Counter modified for aerosol and sheath flow rates of 1 and 10 L min^{-1}, a mobility diameter ($D_{mobility}$) range of 10 to 290 nm, and a sampling period of approximately 3 min. High-frequency total particle number was measured continuously with a TSI 3025A Ultrafine Condensation Particle Counter (UCPC) sampling at 10 Hz. For part of the project, we also obtained a TSI 3045 Aerodynamic Particle Sizer (APS) with an aerodynamic diameter range of 0.4 to 20 μm.

[10] The number concentrations of particles in the 10 to 290 nm range of the DMA ranged from below 10^3 to above 10^4 cm^{-3} with a persistent accumulation mode near 100 nm, as shown in Figure 1. The total particle concentrations measured by the UCPC frequently exceeded 10^5 cm^{-3} and were highly variable. APS measurements of particles with aerodynamic diameter larger than 0.4 μm generally showed fewer particles than in the submicron range. Particles smaller than 20 nm diameter were characterized by large variability in concentration.

2.2. Gas and Particle Phase Chemical Components

[11] In addition to continuous measurements of SO_2, CO, NO_x, and O_3 by AIRMAP (a UNH air quality and climate program, http://airmap.unh.edu) at Appledore Island, CHAiOS measurements included O_3, OIO, and IO by long-path (LP) and multiaxis (MAX) differential optical absorption spectroscopy (DOAS) systems, and volatile organic carbon compounds (VOCs) by proton transfer reaction mass spectroscopy (PTR-MS) and gas chromatography (GC) [*Fischer et al.*, 2006; *Pikelnaya et al.*, 2007; *Hansel et al.*, 1995; *Sive et al.*, 2005; *Zhou et al.*, 2005; *Talbot et al.*, 2005]. Soluble reactive trace gases including HNO_3 [*Fischer et al.*, 2006], NH_3 [*Smith et al.*, 2007], HCl [*Keene et al.*, 2007], and formate and acetate [*Keene et al.*, 2004; *de Gouw et al.*, 2005] were sampled over 2-hour intervals with tandem mist chambers containing deionized water and analyzed within a few hours after recovery by ion chromatography. Size resolved particles were sampled over discrete daytime and nighttime periods with Graseby Anderson cascade impactors configured with polycarbonate substrates and quartz backup filters. After collection, samples were stored frozen, extracted in deionized water, and analyzed at Mount Washington Observatory for major organic and inorganic ionic constituents [*Pszenny et al.*, 2004; *Fischer et al.*, 2006; *Smith et al.*, 2007; *Keene et al.*, 2007].

3. Classification of Nanoparticle Observations

[12] Forty-eight distinct time periods were identified as nanoparticle events, in which particle concentrations for the mode below 80 nm exceeded the intermodal concentrations by a factor of 10 or more for at least 1 hour. The beginning and end of each of these events in which nanoparticle observations persisted are listed with numeric labels as identifiers in Table 1. This section describes the classification of each of these nanoparticle events according to their nanoparticle growth (growth, nongrowth, undetermined), diurnal timing (morning, afternoon, night), and potential gas phase precursor peaks (α- and β-pinene, isoprene, and other precursors).

3.1. Growth During Nanoparticle Events

[13] Of the observed nanoparticle events, half (24) begin with a mode smaller than 20 nm, followed with continuous, or nearly continuous, increases in this modal diameter observed at the Appledore Island tower. These events were identified as "growth" events, and of the other 24 nanoparticle events 14 were classified as "nongrowth." The remaining 10 events are classified as "undetermined," because they included intermittent or poorly separated nanoparticle modes or gaps in the observed nanoparticle mode due to changes in air masses or instrument maintenance. The continuous nature of the observed growth of the nanoparticle mode during the "growth" events is consistent with a photochemical or other time-driven process in an air mass of sufficient regional homogeneity to justify interpretation of the processes in a pseudo-Lagrangian framework. With this assumption, we consider the events as evolving in time with sufficient horizontal homogeneity that the transport term may be neglected.

[14] In the 24 events in which nanoparticles were observed without subsequent growth, nanoparticles may have nucleated from the gas phase but then may have been coagulated, scavenged, or deposited, removing them from the atmosphere before growth could occur. Changes in trajectories or heterogeneities in air masses would also have precluded observing growth had it occurred. Since the probability of observing such a growth event is unknown, it is not possible with this data set to evaluate from the observations the probability that recently nucleated nano-

Table 1. Nanoparticle Events at Appledore Island During ICARTT/CHAiOS 2004, Including Peak Mixing Ratios of Selected Pollutants and Precursors[a]

Event	Date	Start EDT	End EDT	α-Pinene, pptv	β-Pinene, pptv	Isoprene, pptv	NO_x, ppbv	O_3, ppbv	SO_2, ppbv	Transport Region
					Growth With α- and β-Pinene					
4	3 Jul 2004	0700	1700	105.6	133.1	120.9	–	45.9	–	–
5	6 Jul 2004	0545	1030	229.2	170.4	124.9	–	31.1	–	SW-MW
8	7 Jul 2004	0730	1545	137.9	111.0	102.7	–	41.2	–	N
9	10 Jul 2004	0800	1830	89.3	77.7	204.2	6.7	48.8	7.8	NW
13	11 Jul 2004	0730	1930	186.3	186.1	207.9	5.8	35.1	0.4	N
18	17 Jul 2004	0830	0945	101.1	96.9	141.5	4.0	48.8	2.9	NW
19	18 Jul 2004	0545	1700	145.0	206.2	163.8	3.4	73.6	0.5	NW
21	25 Jul 2004	0800	1730	165.3	117.8	101.9	–	50.0	0.6	N
22	26 Jul 2004	0700	1230	214.2	147.3	211.8	–	46.0	5.4	N
25	29 Jul 2004	0900	1630	45.6	27.4	58.4	8.0	46.4	1.7	SW-MW
29	30 Jul 2004	0730	2100	214.9	169.9	559.5	11.8	116.8	2.3	NW-MW-SW
34	2 Aug 2004	0630	2130	208.9	209.6	326.5	3.3	67.9	0.4	NW-MW
35	3 Aug 2004	0800	1400	103.2	58.6	91.8	16.3	117.0	2.3	MW
36	4 Aug 2004	0730	1930	136.9	167.7	171.0	7.8	46.1	0.8	NW-N
38	5 Aug 2004	0930	2130	259.9	203.3	275.2	12.9	38.9	0.3	NW
39	6 Aug 2004	0900	2100	129.8	80.8	146.1	4.4	26.3	0.2	N
40	7 Aug 2004	0815	1615	126.9	80.5	101.9	5.3	14.6	4.9	N
50	10 Aug 2004	0700	1500	71.6	51.5	221.7	15.9	58.7	3.5	NW-MW
Average				148.4	127.5	185.1	8.1	53.0	2.3	
					Other Growth					
1	2 Jul 2004	1930	2230	15.3	20.8	385.5	–	69.8	–	–
12	11 Jul 2004	0030	0830	186.3	186.1	212.7	8.0	34.2	2.5	NW-N
24	28 Jul 2004	0800	1800	5.3	14.9	6.8	4.9	43.3	0.3	M-S
42	7 Aug 2004	2200	0930	53.9	59.0	604.2	8.2	40.9	8.3	N
45	8 Aug 2004	2230	1000	57.4	58.2	212.3	6.2	30.0	17.1	NW
49	9 Aug 2004	2000	0600	42.4	53.0	874.7	12.6	47.0	3.6	NW
Average				60.1	65.3	382.7	8.0	44.2	6.4	
					Nongrowth With Isoprene					
14	11 Jul 2004	1930	2130	14.2	11.6	527.9	6.5	27.2	0.4	N
28	30 Jul 2004	0100	0530	70.5	103.3	559.5	15.2	55.0	4.9	MW-NW
31	31 Jul 2004	0815	2215	19.2	23.2	516.0	12.7	46.0	3.8	SW
32	1 Aug 2004	1230	1630	6.6	7.6	210.0	5.4	39.5	1.2	SW
51	10 Aug 2004	1600	1900	6.7	6.5	186.4	4.2	98.5	1.6	MW
Average				23.4	30.4	400.0	8.8	53.2	2.4	
					Other Nongrowth					
2	3 Jul 2004	0345	0630	105.6	133.1	259.5	–	22.1	–	–
3	3 Jul 2004	0700	0930	97.5	68.3	120.9	–	30.4	–	–
6	7 Jul 2004	0430	0630	137.9	111.0	55.5	–	22.2	–	N
20	25 Jul 2004	0130	0330	111.4	81.2	106.7	–	23.6	0.2	N
26	29 Jul 2004	1530	1630	5.0	2.9	46.2	7.2	36.6	1.7	MW
30	30 Jul 2004	1950	2130	–	–	129.6	5.2	88.3	0.7	SW
37	4 Aug 2004	2100	0830	259.9	203.3	408.5	10.4	26.0	1.7	NW
43	8 Aug 2004	0945	1115	26.0	14.1	65.7	9.0	40.9	3.4	NW
44	8 Aug 2004	1330	1730	27.9	30.7	160.0	5.1	42.3	1.3	NW
Average				96.4	80.6	150.3	7.4	36.9	1.5	
					Undetermined					
7	7 Jul 2004	0730	0345	110.5	85.2	106.5	–	41.2	–	N-S
10	10 Jul 2004	0900	1130	37.5	23.2	199.7	5.9	37.2	7.8	NW
11	10 Jul 2004	1930	0830	186.3	186.1	212.7	8.0	48.5	2.5	NW-N
15	12 Jul 2004	1030	1300	18.0	27.7	527.9	20.1	37.6	3.9	N-S
16	12 Jul 2004	1030	1700	24.0	11.3	43.5	12.7	41.1	3.9	S
17	15 Jul 2004	1900	1000	101.1	96.9	283.6	10.5	85.0	3.5	M-SW-MW
23	28 Jul 2004	0115	0800	6.4	29.3	39.2	7.3	36.9	1.3	N-M
33	1 Aug 2004	1600	0800	208.4	209.6	1047.2	7.3	39.5	1.0	SW-MW-NW
46	9 Aug 2004	0545	1445	56.4	43.6	199.4	5.0	32.1	16.9	NW
48	9 Aug 2004	1600	0700	42.4	53.0	874.7	12.6	47.0	3.6	NW
Average				79.1	76.6	353.4	9.9	44.6	4.9	

[a]The table describes the 48 nanoparticle events, numbered nonconsecutively from 1 to 51, omitting 27, 41, and 47. "Growth with α- and β-pinene" events are categorized on the basis of the presence of α- and β-pinene peaks preceding the event, for which the average mixing ratios are reported; isoprene mixing ratios are also reported as peak averages for "nongrowth with isoprene" events. Entries in the table were indicated as dashes if values were not measured for the event (including both values below detection or instrument maintenance events). The remaining three categories ("other growth," "other nongrowth," and "undetermined") did not exhibit identifiable peaks, and average ambient mixing ratios are reported. Events 3 and 4 begin at the same time and refer to two separate nanoparticle modes: Event 3 is the "nongrowth" of the 60 nm mode, and event 4 is the "growth" of the 20 nm mode. O_3 for 3–7 July are provided by AIRMAP; other O_3 mixing ratios including all averages calculated use only measurements by DOAS.

particles (<20 nm) will grow. Instead the common features of the growth events are used to distinguish the necessary or sufficient conditions for nanoparticles (~20 nm) to grow from conditions in which no growth is observed.

3.2. Diurnal Timing of Nanoparticle Events

[15] Many (19) of the 24 nanoparticle growth events started shortly after sunrise and low tide, with start times ranging between 0545 and 0930 local time (EDT), an observation similar to *Wehner et al.* [2005]. The average duration of these events is about 9 hours 45 min, with extremes of 4 hours 45 min and 13 hours 30 min. The remaining 5 nanoparticle growth events occurred in the evening or nighttime hours, possibly associated with subsidence of growing particles from the free troposphere [*Russell et al.*, 1998] or polluted air masses containing nitrogen oxides or other compounds that react without sunlight. The morning events were more frequent, occurring during 19 of the 40 sampling days. Eighteen of these 19 morning events are identified by event number in Figure 1, with 12 highlighted by symbols overlying the measured size distributions to show the fitted modal mean diameter and highlight the observed increase in particle diameter. The numeric labels correspond to the numeric event identifiers in Table 1.

3.3. Potential Gas Phase Precursors With Peak Mixing Ratios Preceding Nanoparticle Events

[16] The only effective atmospheric process for nanoparticle growth that can account for the observed changes in particle diameter is condensation of gas phase species, possibly as a result of photochemical oxidation of primary emissions into more oxidized compounds with lower vapor pressures. Table 1 reports the maximum concentration for each event for several key gas phase pollutants, including SO_2, NO_x, and O_3. No clear distinction was seen between the nanoparticle events that included growth and those that did not for these pollutants.

[17] The top plot for each week of data in Figure 1 includes time series of mixing ratios for O_3 and α- and β-pinene. This plot shows that almost all (18 of 19 morning growth events) of the frequent morning growth events were preceded by high diurnal maxima in both α- and β-pinene. This diurnal cycle of a morning peak in α- and β-pinene mixing ratios differs from the isoprene pattern at this site, since the isoprene emissions typically peak later in the day. The events with these peaks preceding particle growth are categorized in Table 1 as "growth with α- and β-pinene" to distinguish them from the remaining six "other growth" events. For the nongrowth events another trend is evident in Table 1, namely the high isoprene mixing ratios preceding the five "nongrowth with isoprene" events. There are nine "other nongrowth" events without high isoprene mixing ratios. This classification of nanoparticle events by gas phase precursors is based on the peaks occurring before the events, with average mixing ratios given in Table 1. The average mixing ratio was sometimes high when no peak was observed: event 12 is classified as "other growth" despite its high average mixing ratios of α- and β-pinene, and events 2 and 37 were classified as "other nongrowth" despite a high average mixing ratio of isoprene. Tables 2a and 2b show gas phase precursor mixing ratios for each of these types of events.

[18] For the nanoparticle "growth with α- and β-pinene" events, peak α- and β-pinene mixing ratios varied from 51 to 260 pptv, with diurnal maxima occurring 1 to 3 hours before the nanoparticle appearance. For these events, the average mixing ratios for the peaks preceding the events were 148 for α-pinene and 128 pptv for β-pinene. At the beginning of the nanoparticle growth events, α- and β-pinene mixing ratios decreased. Just before the events, the maxima in α- and β-pinene mixing ratios were usually accompanied by minima in ozone mixing ratios, consistent with oxidation of α- and β-pinene by consuming photochemically produced ozone. Ozone itself follows a similar pattern with slight time offset, typically peaking at a maximum value near 53 ppbv then dropping rapidly down to the project and event average of 36 ppbv. Other mechanisms are also likely to contribute to primary and secondary products from α- and β-pinene oxidation as photo and NO_3 oxidation have been shown to have comparable yields [*Odum et al.*, 1996; *Hoffmann et al.*, 1997; *Griffin et al.*, 1999; *Yu et al.*, 1999; *Hoppel et al.*, 2001; *Cocker et al.*, 2001; *Presto et al.*, 2005b; *Presto and Donahue*, 2006].

[19] Most of the "other growth" events have high values of NO_x, O_3, and SO_2 relative to project means. Event 45 has the highest SO_2 mixing ratios, exceeding 17 ppbv at peak, whereas other events have average concentrations between 2 and 8 ppbv. These events occur at various times of day with one beginning in the morning (0800 EDT), one in the early evening (1930 EDT), and three events late at night (between 2000 and 0030 EDT). Neither group of nanoparticle growth events had elevated levels of iodine oxides, with average mixing ratios for both growth categories falling within 30% of the project mean mixing ratios for OIO and IO (as listed in Tables 2a and 2b).

[20] Tables 2a and 2b highlight other chemical distinctions among these five categories of nanoparticle events by comparing the average of the maximum values during each type of event to the project mean value. For the nanoparticle "growth with α- and β-pinene" events, the peaks in α- and β-pinene mixing ratios of 15 of these 18 events are more than twice the project mean mixing ratios of 30 and 31 pptv, respectively. In addition, a number of other measured VOCs have high mixing ratios during these events, including propane, i-pentane, n-pentane, 2-methylpentane, 3-methylpentane, 2,2,4-trimethylpentane, 2,3,4-trimethylpentane, tetrachloroethene, and trichloroethene. Several VOCs are also high during other categories of nanoparticle events, with those with mean values more than 30% higher than the project mean and those with maximum values exceeding twice the mean appearing in bold typeface. The "growth with α- and β-pinene" events also have higher average and maximum NO, HNO_3, HCl, and NH_3 mixing ratios than the project mean. For the "growth with α- and β-pinene" events, the chemical composition of supermicron and submicron particles is typical for the project, with the category average never more than 30% higher than the project mean. There are occasionally high particle concentrations of methane sulfonate, sulfate, iodide, nitrate, and ammonium, as their maximum values during some of the "growth with α- and β-pinene" events are more than twice the project mean. The high sulfate is consistent with some influence in the supermicron particles of high-sulfur fossil fuel combustion emissions.

Table 2a. Mean and Maximum Mixing Ratios of Gas Phase Chemical Constituents During Nanoparticle Events at Appledore Island During ICARTT/CHAiOS 2004[a]

	Project	Growth With α- and β-Pinene		Other Growth		Nongrowth With Isoprene		Other Nongrowth		Undetermined	
	Mean	Mean	Maximum	Mean	Maximum	Mean	Maximum	Mean	Maximum	Mean	Maximum
Carbon monoxide, ppbv	172	193	231	175	214	197	218	174	191	174	223
Nitrogen oxide, ppbv	1	**2**	**4**	0	**2**	0	1	**1**	**3**	**1**	**3**
Nitrogen oxides (NO_x), ppbv	4	4	8	4	8	**5**	**9**	**5**	7	**5**	**10**
Ozone, ppbv	36	36	53	27	44	38	53	28	37	27	45
Sulfur dioxide, ppbv	1	1	2	**2**	**6**	1	**2**	1	1	**2**	**5**
Iodine dioxide, pptv	19	13	22	10	17	12	13	15	20	12	18
Iodine oxide, pptv	4	3	5	4	5	**5**	7	4	5	3	6
Hydrogen chloride, pptv	602	**769**	**1333**	175	427	**905**	1047	**736**	964	594	**1398**
Acetic acid, pptv	494	563	702	457	614	507	592	586	660	501	698
Formic acid, pptv	739	858	1107	548	768	814	923	842	964	716	1084
Nitric acid, pptv	828	1030	1463	302	486	1040	1112	**1391**	**1676**	592	979
Ammonia, pptv	440	**603**	**1047**	413	596	233	261	378	438	409	847
Ethane, pptv	1077	1175	1503	971	1171	1098	1254	1171	1439	1062	1482
Ethene, pptv	230	295	**547**	278	**517**	**371**	**471**	**314**	**479**	280	**550**
Ethyne, pptv	332	394	664	311	540	**495**	645	380	544	337	569
Propane, pptv	783	**1160**	**2186**	861	1395	857	1091	**1100**	**1792**	772	1520
Propene, pptv	52	64	**136**	–	–	–	–	–	–	67	**159**
i-butane, pptv	72	79	**167**	–	–	–	–	–	–	87	**180**
n-butane, pptv	123	161	**376**	–	–	–	–	–	–	145	**344**
1-butene, pptv	10	12	**26**	–	–	–	–	–	–	12	**31**
Cyclopentane, pptv	9	10	**21**	–	–	–	–	–	–	9	**21**
i-pentane, pptv	166	**259**	**590**	–	–	–	–	–	–	201	**515**
n-pentane, pptv	66	**96**	**210**	–	–	–	–	–	–	84	**198**
Methylcyclopentane, pptv	35	36	**71**	–	–	–	–	–	–	35	**71**
2,2-dimethylbutane, pptv	12	13	**26**	–	–	–	–	–	–	13	24
Cyclohexane, pptv	15	17	**40**	–	–	–	–	–	–	19	**45**
2-methylpentane, pptv	47	**63**	**137**	–	–	–	–	–	–	57	**138**
3-methylpentane, pptv	38	**52**	**108**	–	–	–	–	–	–	**53**	**117**
n-hexane, pptv	37	42	**84**	–	–	–	–	–	–	45	**93**
n-heptane, pptv	19	22	**48**	–	–	–	–	–	–	22	**51**
n-octane, pptv	11	11	**24**	–	–	–	–	–	–	12	**27**
n-nonane, pptv	9	9	18	–	–	–	–	–	–	10	**20**
n-decane, pptv	14	13	22	–	–	–	–	–	–	16	**31**
Isoprene, pptv	84	59	**185**	**201**	**383**	**129**	**359**	93	150	**139**	**353**
2,4-dimethylpentane, pptv	12	–	–	–	–	–	–	–	–	13	**31**
2,3-dimethylpentane, pptv	11	13	**33**	–	–	–	–	–	–	12	**32**
Methylcyclohexane, pptv	13	–	–	–	–	–	–	–	–	13	**28**
2,2,4-trimethylpentane, pptv	39	**53**	**141**	–	–	–	–	–	–	47	**134**
2,3,4-trimethylpentane, pptv	11	**14**	**42**	–	–	–	–	–	–	12	**32**
Benzene, pptv	78	74	116	–	–	–	–	–	–	88	144
Toluene, pptv	136	166	**336**	–	–	–	–	–	–	166	**348**
Ethylbenzene, pptv	21	21	**47**	–	–	–	–	–	–	23	**48**
m, p-xylene, pptv	92	89	166	–	–	–	–	–	–	102	**185**
o-xylene, pptv	27	28	52	–	–	–	–	–	–	27	47
1,2,4-trimethylbenzene, pptv	20	–	–	–	–	–	–	–	–	19	40
α-pinene, pptv	30	**43**	**114**	**46**	**71**	7	12	**55**	**96**	**52**	**112**
β-pinene, pptv	31	37	**98**	**43**	**75**	7	12	**53**	**92**	–	–
Camphene, pptv	20	–	–	19	29	–	–	26	40	–	–
Limonene, pptv	8	–	–	–	–	–	–	**10**	15	–	–
Carbonyl sulfide, pptv	404	372	414	359	379	435	470	374	390	369	415
Methyl chloride, pptv	515	516	548	498	526	505	549	505	523	500	538
Methyl bromide, pptv	8	8	9	8	9	8	8	8	8	8	9
Methyl iodide, pptv	1	1	1	1	1	2	2	1	1	1	1
Dichloromethane, pptv	47	54	72	41	51	59	74	50	60	43	59
Chloroform, pptv	21	25	32	21	25	22	25	23	28	21	26
Trichloroethene, pptv	8	**11**	**29**	5	13	**17**	30	8	**21**	6	**24**
Tetrachloroethene, pptv	22	**29**	**53**	18	25	**32**	41	25	32	20	34
Dibromomethane, pptv	3	2	4	2	3	4	5	3	3	2	3
Bromoform, pptv	14	10	18	8	12	**21**	27	12	17	9	16
Ethyl iodide, 10^3 pptv	46	28	69	22	33	**62**	77	29	38	21	54
Chloroiodomethane, pptv	1	0	1	0	1	1	1	1	1	0	1
Methyl nitrate, pptv	3	3	3	2	3	3	3	3	3	3	3
Ethyl nitrate, pptv	3	3	4	2	3	3	4	3	3	2	3
2-propyl nitrate, pptv	10	10	15	6	8	10	12	8	9	7	11
1-propyl nitrate, pptv	1	1	2	1	1	1	2	1	1	1	2
2-butyl nitrate, pptv	7	7	12	4	6	7	9	5	7	4	8
3-pentyl nitrate, pptv	2	2	**4**	1	2	2	3	2	2	1	3
2-pentyl nitrate, pptv	3	3	**5**	2	2	3	5	2	3	2	4
Methanol, pptv	2230	**2996**	3886	**3862**	**5105**	2133	2827	**3101**	3662	2869	**4471**

Table 2a. (continued)

	Project Mean	Growth With α- and β-Pinene		Other Growth		Nongrowth With Isoprene		Other Nongrowth		Undetermined	
		Mean	Maximum	Mean	Maximum	Mean	Maximum	Mean	Maximum	Mean	Maximum
Acetaldehyde, pptv	433	533	743	522	735	494	620	503	626	499	768
Acetone, pptv	1454	1825	2151	1796	2134	1480	1751	1631	1907	1565	2090
Methyl ethyl ketone, pptv	168	212	304	163	258	206	259	170	212	189	319
Methyl vinyl ketone + methacrolein, pptv	207	236	**474**	**373**	**618**	**425**	**666**	**315**	402	**352**	**683**
Terpenes (total), pptv	92	**138**	**395**	**127**	**184**	51	66	**164**	**240**	98	**260**
Acetonitrile, pptv	106	114	133	135	164	109	119	107	120	125	165
C8 aromatics, pptv	95	110	**219**	**133**	**239**	89	132	**145**	**210**	**131**	**235**
C9 aromatics, pptv	70	75	**142**	90	**165**	69	100	**96**	131	**92**	**156**
Dimethyl sulfide, pptv	48	26	48	27	52	41	50	35	53	35	59

[a]Values listed in boldface indicate that the category mean exceeds the project average by 30% or that the category maximum is more than double the project average. Measured compounds were omitted and entries in the table were indicated as dashes if values were not available during more than half of each event or for more than half of the events (including both values below detection or instrument maintenance events). For gas phase components, the maximum for each category represents the average of the maximum for each event in that category. O_3 for 3–7 July are provided by AIRMAP; other O_3 mixing ratios including all averages calculated use only measurements by DOAS. Note that Table 2 reports the mean mixing ratios during the events, excluding preceding peak values, and consequently differs from the values reported in Table 1 which include preceding peaks.

[21] All of the nanoparticle event categories have a maximum mixing ratio of isoprene that is more than twice the project mean isoprene mixing ratio. In addition, the "nongrowth with isoprene" events have peaks in isoprene. SO_2, NO_x, ethane and methyl vinyl ketone + methacrolein have maximum mixing ratios that exceed twice the project average for the "nongrowth with isoprene." These nanoparticles typically occurred with modal diameters between 30 and 60 nm, with the mode persisting for 5 hours at the Appledore Island tower site in the afternoon or evening. The

Table 2b. Mean and Maximum Concentrations and Levels of Particle Phase Chemical Constituents During Nanoparticle Events at Appledore Island During ICARTT/CHAiOS 2004[a]

	Project Mean	Growth With α- and β-Pinene		Other Growth		Nongrowth With Isoprene		Other Nongrowth		Undetermined	
		Mean	Maximum	Mean	Maximum	Mean	Maximum	Mean	Maximum	Mean	Maximum
Supermicron particles											
Oxalate, 10^{-3} nmol m^{-3}	196	119	391	77	143	234	**397**	139	**518**	196	375
Methane sulfonate, 10^{-3} nmol m^{-3}	61	26	**136**	20	67	**109**	**185**	61	**196**	58	**260**
Sulfate, nmol m^{-3}	9	6	**26**	3	8	**12**	**43**	10	**26**	6	**18**
Chloride, nmol m^{-3}	19	12	25	14	20	22	**50**	16	25	20	**56**
Bromide, 10^{-3} nmol m^{-3}	25	18	33	21	26	27	**53**	**32**	**92**	28	**73**
Iodide, 10^{-3} nmol m^{-3}	3	2	**8**	0	1	**3**	**7**	2	**8**	1	4
Nitrate, nmol m^{-3}	10	9	**22**	2	4	**15**	**24**	12	**32**	11	**39**
Ammonium, nmol m^{-3}	8	6	**38**	1	3	**13**	**51**	**10**	**38**	3	13
Sodium, nmol m^{-3}	24	15	31	13	19	**34**	**71**	22	**49**	24	**74**
Potassium, nmol m^{-3}	1	1	1	0	1	**1**	**2**	**1**	**2**	**1**	**2**
Magnesium, nmol m^{-3}	3	2	4	2	2	**4**	**8**	3	**6**	3	**9**
Liquid water content, nL m^{-3}	11.9	4.2	14	3	11	11	**34**	6	16	5	16
Submicron particles											
Acetate, 10^{-3} nmol m^{-3}	150	138	**558**	87	258	**204**	**383**	96	295	103	214
Formate, 10^{-3} nmol m^{-3}	285	295	**956**	159	534	362	**784**	190	**873**	216	515
Oxalate, 10^{-3} nmol m^{-3}	107	100	**350**	124	**362**	103	**340**	131	**350**	128	**411**
Methane sulfonate, 10^{-3} nmol m^{-3}	102	79	**232**	65	**252**	**142**	**214**	69	**237**	54	**258**
Sulfate, nmol m^{-3}	13	12	**47**	4	10	15	**35**	6	**51**	6	24
Chloride, 10^{-3} nmol m^{-3}	79	61	**454**	7	15	48	80	131	**454**	51	**527**
Bromide, 10^{-3} nmol m^{-3}	10	8	**22**	11	**39**	11	17	4	**24**	5	15
Iodide, 10^{-3} nmol m^{-3}	4	**5**	**10**	3	**12**	4	**9**	3	**10**	2	6
Nitrate, nmol m^{-3}	1	1	**4**	0	0	1	**2**	1	**4**	0	**2**
Ammonium, nmol m^{-3}	18	18	**58**	5	7	21	**47**	11	**84**	10	51
Sodium, 10^{-3} nmol m^{-3}	415	295	484	136	188	**797**	**1720**	274	806	307	**1909**
Potassium, 10^{-3} nmol m^{-3}	127	106	240	153	**436**	134	**432**	77	117	**196**	**460**
Magnesium, 10^{-3} nmol m^{-3}	67	49	114	58	126	**110**	**208**	41	109	73	**182**
Liquid water content, nL m^{-3}	6.6	4.1	**25.4**	1.3	5.0	7.2	**28.7**	2.2	12.2	1.4	7.2
pH	1.1	1.1	–	**1.6**	–	0.9	–	**1.4**	–	**1.5**	–

[a]Note that Table 2 reports the mean mixing ratios during the events, excluding preceding peak values, and consequently differs from the values reported in Table 1 which include preceding peaks. Values listed in boldface indicate that the category mean exceeds the project average by 30% or that the category maximum is more than double the project average. Measured compounds were omitted and entries in the table were indicated as dashes if values were not available during more than half of each event or for more than half of the events (including both values below detection or instrument maintenance events). For particle phase components, the measurement resolution included only one measurement per event, and so the reported values are the maxima of all events for that category.

α- and β-pinene mixing ratios did not have prominent peaks preceding these events. In addition, the submicron particle concentrations of acetate and formate and the supermicron concentrations of sulfate, nitrate, and ammonium exceed the project averages by more than 30%. Another important particle characteristic during the "nongrowth with isoprene" events is the high concentration of methane sulfonate in the submicron and supermicron particle sizes, since this organosulfate could be consistent with the oxidation and sulfate esterification of isoprene suggested by a number of recent studies [*Edney et al.*, 2005; *Kroll et al.*, 2005; *Jaoui et al.*, 2005; *Surratt et al.*, 2006; *Liggio and Li*, 2006; *Kleindienst et al.*, 2006; *Gao et al.*, 2006]. The high mean and peak mixing ratios of methyl vinyl ketone + methacrolein during the "nongrowth with isoprene" events could also suggest that a large fraction of the isoprene oxidation products may remain in the gas phase. The limited number of these events during the CHAiOS study do not support further speculation on isoprene SOA formation at this time, although they suggest the need for a study with expanded scope that includes chemical measurements of SOA tracers in the nanoparticle size range.

4. Discussion of Nanoparticle Growth Events With Preceding Pinene Peaks

[22] For the 18 nanoparticle "growth with α- and β-pinene" events, HYPSLIT back trajectories were calculated each hour during the event. A trajectory initialized at 100 m during the middle of each event is shown in Figure 2. Fifteen of the 18 nanoparticle "growth with α- and β-pinene" events occurred during times when the air masses originated from the midwest and northeast regions, falling into two transport categories, namely, northwest (NW) (Figure 2a) and north/northeast (NNE E Canada) (Figure 2b). Figure 2 shows that trajectories in these two categories frequently incorporated long paths over forested regions in Vermont, Maine, and western Massachusetts, respectively, as well as in eastern Canada and northern New York and New Hampshire. The remaining three events 5, 25, and 35 (shown in Figure 2c) involved flow from the Midwest (MW) or southwest (SW) urban sectors. These regional transport sectors are consistent with a widely distributed source such as pine forests, occurring in several of the regional transport sectors.

[23] The growth of the nanoparticle mode observed at Appledore Island can be quantified in two ways. First, the observed change in the modal peak (and number mean for a lognormal mode fit) diameter provides a characteristic rate of change based on all contributing growth processes. This particle mode peak growth rate is directly observed as the slope of the modal diameter with time, and for condensation to particles in the kinetic regime the rate of mass transfer results in diameter increases that are linear in time [*Seinfeld and Pandis*, 1998; *Birmili et al.*, 2003]. Second, if we identify the condensing vapor or its precursor, the aerosol mass fraction or yield can be calculated as the increase in particle mass that accompanies the observed decrease in one or more probable precursor gases. Because the assignment of the latter precursor gases is tentative and incomplete, the calculations should be seen as an "effective" yield and an upper bound for the ambient mixture of precursors. For the 18 "growth with α- and β-pinene" events observed in this study, we have chosen to focus on the apparent yield inferred from α- and β-pinene oxidation as it seems to be the most probable candidate [*Odum et al.*, 1996; *Hoffmann et al.*, 1997; *Griffin et al.*, 1999; *Yu et al.*, 1999; *Hoppel*

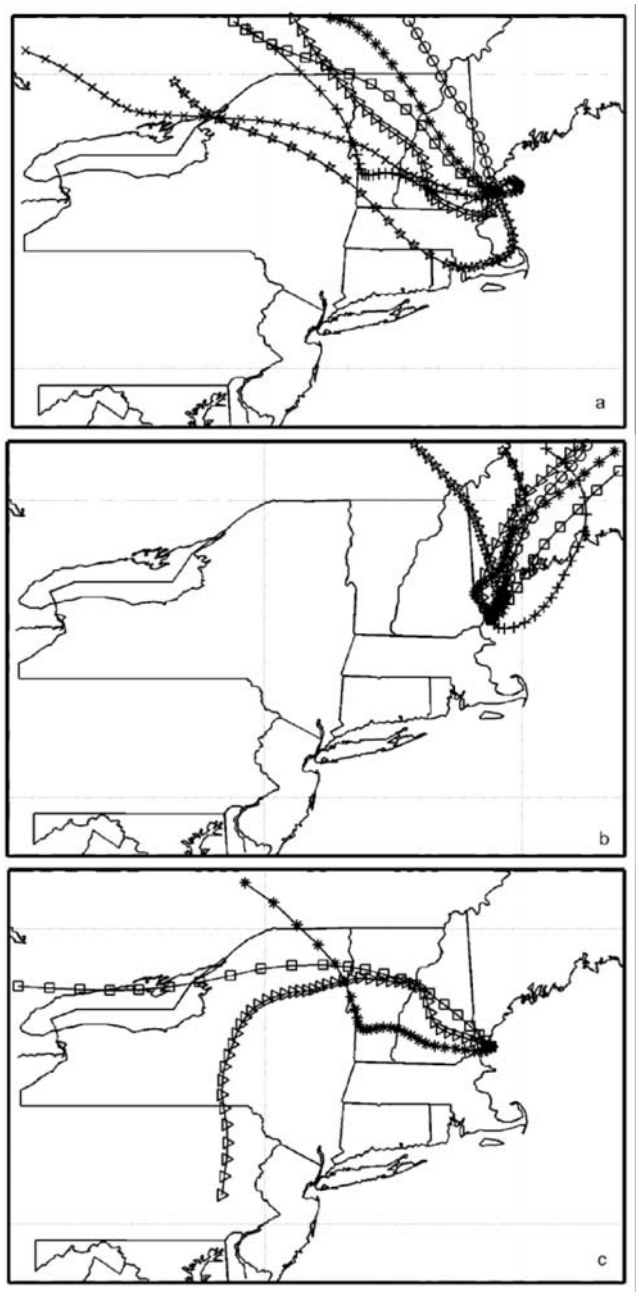

Figure 2. Representative air mass back trajectories for the morning nanoparticle growth event with high α- and β-pinene concentrations. These 24 hour trajectories were initialized near the middle of each event, and markers indicate time steps of 1 hour. The categories are (a) NW, (b) NNE and E Canada, and (c) MW and SW urban. Figure 2a shows events 9 (squares), 29 (triangles), 18 (asterisks), 4 (circles), 35 (pluses), 50 (crosses), and 19 (five-point stars). Figure 2b shows events 21 (squares), 40 (triangles), 22 (asterisks), 39 (circles), 38 (pluses), 8 (crosses), 13 (five-point stars), and 36 (six-point stars). Figure 2c shows events 5 (squares), 25 (triangles), and 35 (asterisks).

et al., 2001; *Presto et al.*, 2005a, 2005b; *Lee et al.*, 2006]. Both approaches, namely comparing the growth rates to other field measurements of observed nanoparticle growth and comparing the yields to laboratory studies of yield for individual precursors, provide important measures of how these nanoparticle events relate to prior ambient and laboratory observations.

4.1. Observed Nanoparticle Growth Rates

[24] Of the 18 "growth with α- and β-pinene" events, 12 were sufficient for lognormal fits during the growth event. Examples of the lognormal fits to the nanoparticle modes at the start and end of each event are illustrated for these 12 events in Figure 3. Since each event lasted 5 hours or longer, more than 100 modal diameters were obtained and fit by linear regression to provide a growth rate [*Kulmala et al.*, 2004]:

$$GR = \frac{\Delta D_{\mathrm{mode}}}{\Delta t}\left[\mathrm{nm\,h^{-1}}\right].$$

where GR is the growth rate in nm h^{-1}, D_{mode} is the mean diameter of the mode in nm, and t is the time in hours (h). The average diameter growth rate for events with high α- and β-pinene mixing ratios is 6.6 nm h^{-1}, ranging from 3.3 to 13.2 nm h^{-1}.

[25] The growth rates for 11 of the 18 "growth with α- and β-pinene" events are shown in Figure 4. Growth rates were not determined for the remaining growth events because those events included gaps in measurements for more than 20% of the event duration or did not have distinguishable beginning and ending particle modal diameters. For example, the nanoparticle growth rate could not be calculated for event 22 because the nanoparticle mode at the end of the event could not be distinguished from the preexisting accumulation mode at 100 nm.

[26] Other studies that report growth rates (or from which growth rates have been estimated [*Kulmala et al.*, 2004]) report values from 1 to 20 nm h^{-1}. Exceptionally high growth rates of up to 200 nm h^{-1} are reported from the PARFORCE study [*O'Dowd et al.*, 2002; *Dal Maso et al.*, 2002]. The high average growth rates observed during summer at Appledore Island are consistent with the annual pattern found in the HAFEX study [*Birmili et al.*, 2003] and in Hyytiälä [*Mäkelä et al.*, 2000b]. Several reported nanoparticle growth rates for forested and other rural continental studies are summarized in Figure 4. The values observed at Appledore Island are consistent with the range reported in the literature. One interesting note is that the estimated growth rates and associated ozone mixing ratios from published nanoparticle observations show no clear trend in the observed rate of growth with ozone mixing ratio, a relationship that might be expected if precursors were abundant and the primary oxidant was ozone. During the "growth with α- and β-pinene" events reported here, there is a weak trend (satisfying a t-test at the 90% confidence level) consistent with ozone being one of several oxidants.

[27] In contrast to the results of *Birmili et al.* [2003] and *Held et al.* [2004], the observed growth rates are approximately linear and constant throughout the duration of the events. This linear increase in particle diameter is often associated with a regional event [*Kulmala et al.*, 2004] and a constant concentration of condensable vapor for particles small enough to have kinetic-regime mass transfer processes [*Seinfeld and Pandis*, 1998].

4.2. Apparent Nanoparticle Aerosol Mass Fraction (Yield) From Photochemical α- and β-Pinene Oxidation

[28] The correlation of three quarters of the nanoparticle growth events observed with peaks in α-pinene and β-pinene followed by their apparent consumption in photochemical atmospheric oxidation reactions provides a substantial justification for considering the apparent yield of nanoparticle mass from α- and β-pinene oxidation, even though there are certainly a wide variety of other contributing or potential precursors. Several other hydrocarbons are present at high concentrations during these events, but they lacked the pattern of peaks-followed-by-decreases which provides less evidence for gas-to-particle conversion and implies that their contribution to condensed mass is less significant than that of α- and β-pinene. Other precursors cannot be ruled out, and several compounds are good candidates for cocondensates (in particular NH_3), so the calculated aerosol mass fractions (yields) are upper bounds that may incorporate the effects of other unidentified gas phase precursors on the observed atmospheric yields of aerosol. The aerosol produced is nominally SOA, although ammonium and other species that partition or react from the gas phase also may contribute inorganic components to the additional aerosol mass.

[29] Following the approach of *Odum et al.* [1996], the secondary organic aerosol yield is

$$Y = \frac{\Delta M_0}{\Delta ROG}$$

where ΔM_0 is the increase in particle mass and ΔROG is the decrease in reactive organic gases, which is equivalent to an aerosol mass fraction (AMF) [*Presto and Donahue*, 2006]. Estimating the aerosol mass fraction (yield) for field observations is more appropriately identified here as an apparent nanoparticle aerosol mass fraction (AMF_n) since mass increases to larger particles are small relative to the preexisting mass and could not be quantified from the mobility-based exponential-sizing of the DMA. For this reason, we specify that here we calculate only

$$AMF_n = \frac{\Delta M_{0,n}}{\Delta ROG}$$

where $\Delta M_{0,n}$ is the change in mass for the nanoparticle mode located at diameters smaller than 100 nm. $\Delta M_{0,n}$ was calculated from the observed final nanoparticle mass, subtracting the initial nanoparticle mass and requiring constant number concentrations. The lognormal fits used for this calculation are shown in Figure 3. The changes in number concentration during each event are most likely associated with some degree of heterogeneity in the air mass, for which we cannot correct in the Eulerian framework of these measurements. The resulting estimate is a lower bound accounting only for the growth from the size first observed and for the particle number that remain at the end. ΔROG is the sum of the decrease in α- and β-pinene.

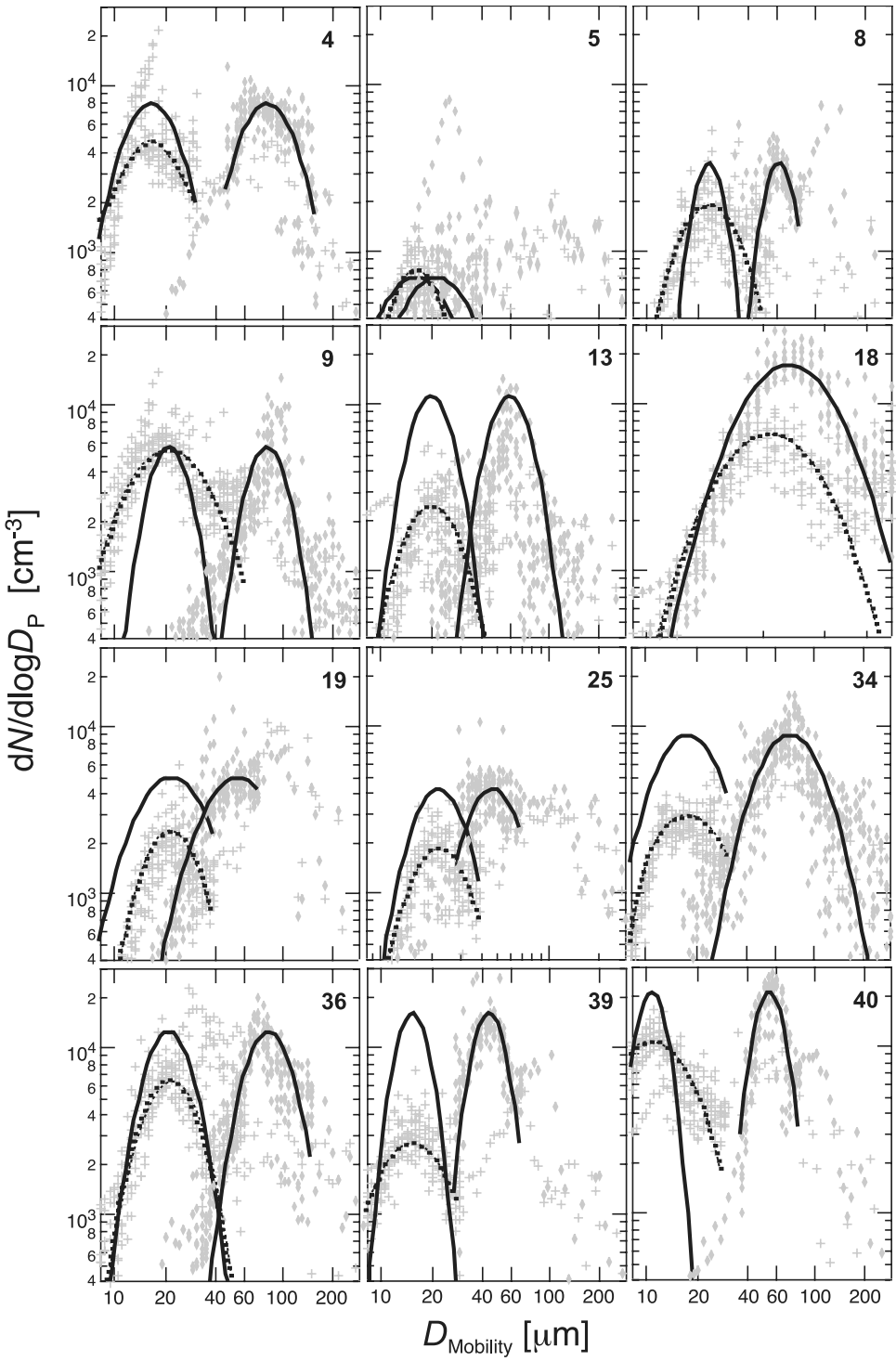

Figure 3. Particle size distributions and lognormal fits for the start and end of nanoparticle growth events. Symbols show ten measured size distributions at the start and end of each event. The dashed line shows a curve fit to the nanoparticle mode at the beginning of the event, and the solid line on the right shows the nanoparticle mode at the end of each event. The solid line on the left of each distribution shows the initial nanoparticle mode used to estimate the lower bound on the particle yield if each event were Lagrangian and number-conserving (the inferred initial nanoparticle mode fit is omitted for event 18 since the growth was insufficient for a calculation of the yield).

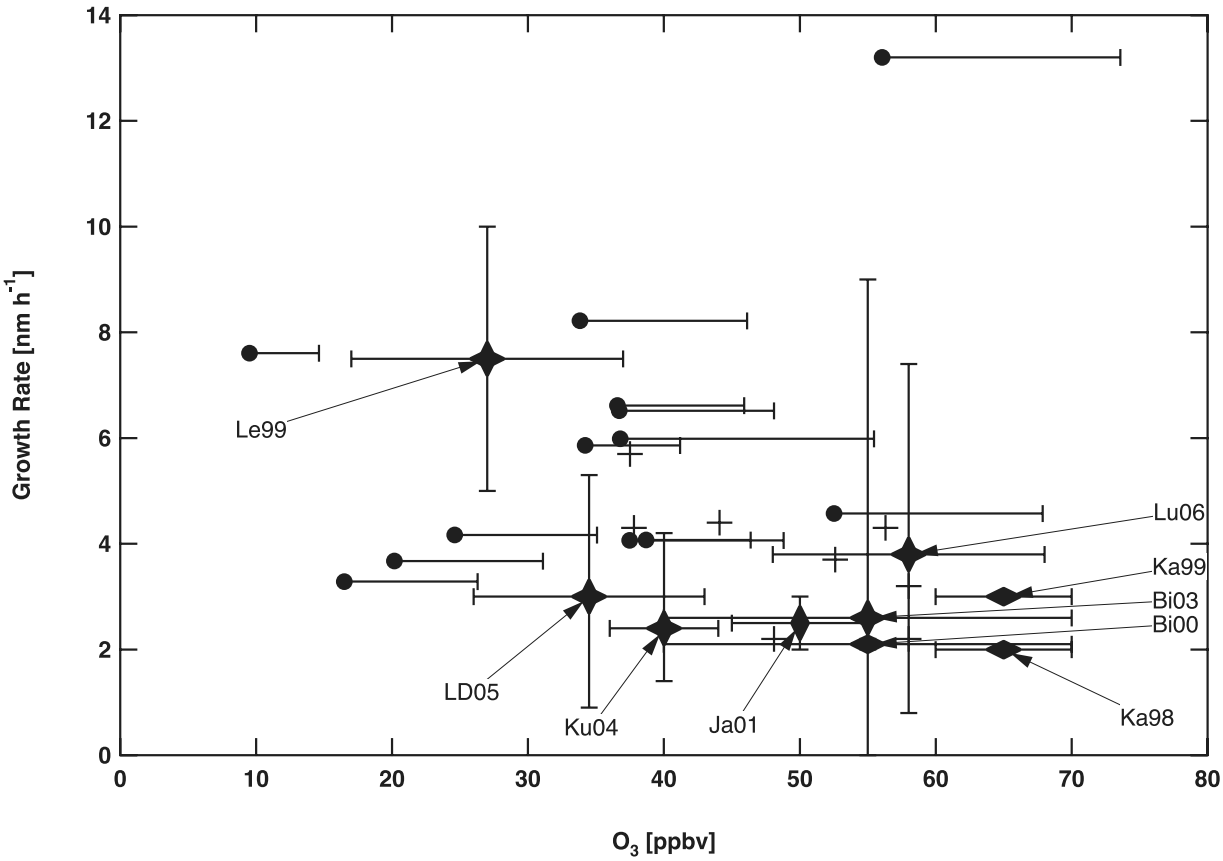

Figure 4. Growth rates and ozone mixing ratios for forest-influenced nanoparticle observations. Solid circles report the mean values for each nanoparticle "growth with α- and β-pinene" event, with whiskers marking the peak ozone value measured during the events. Pluses show results from *Held et al.* [2004]. Other observations of nanoparticle growth rates are marked by the first two letters and the year, with whiskers giving the range or standard deviation, as reported: Le99 [*Leaitch et al.*, 1999], LD05 [*Lyubovtseva et al.*, 2005; *Dal Maso et al.*, 2002], Ku04 [*Kulmala et al.*, 2004], Ja01 [*Janson et al.*, 2001], Lu06 [*Lunden et al.*, 2006], Ka99 [*Kavouras et al.*, 1999], Bi03 [*Birmili et al.*, 2003], Bi00 [*Birmili et al.*, 2000], and Ka98 [*Kavouras et al.*, 1998].

[30] The resulting values of increase in nanoparticle mode mass range from 0.001 to 2 μg m^{-3} for nanoparticle yields between 0.0005 and 1, as shown in Figure 5. As is expected from the *Odum et al.* [1996] model, there is a correlation between yield and SOA increase. This relationship appears to hold for the nanoparticle mode observed at Appledore Island, consistent with the explanation that the condensed organic oxidation products play a role in gas-particle partitioning by absorption. The correlation is surprisingly tight for field observations, with a slope of nearly 0.5 and an R^2 value of 0.85. There is also a distinction between the events (13, 34, 36, 9, 4) in which the nanoparticle AMF may dominate the overall SOA yield because there are very few accumulation-mode particles to act as a sink from those events for which there was a much higher concentration of particles between 100 and 300 nm diameter (25, 8, 19, 39, 40). The apparent AMF to the nanoparticles is higher when there are fewer accumulation mode particles present to provide a large preexisting particle surface area.

[31] Laboratory measurements of α- and β-pinene oxidation with O_3, NO_3, and OH provide a relevant comparison, as they have been used as the basis to estimate SOA production at Appledore Island and globally [*Kanakidou et al.*, 2000]. Companion ICARTT/CHAiOS papers indicate that atomic Cl was present in coastal New England air at significant concentrations during daytime (>10^4 cm^{-3}), which would have contributed to the oxidation of α- and β-pinene [*Keene et al.*, 2007; *Pszenny et al.*, 2007]. This potential contribution from halogens has been quantified in controlled conditions [*Cai and Griffin*, 2006]. Figure 5 summarizes the reported α- and β-pinene oxidation yields at temperatures ranging between 20°C and 40°C reported for several independent sets of measurements [*Hoffman et al.*, 1997; *Griffin et al.*, 1999; *Yu et al.*, 1999; *Odum et al.*, 1996; *Presto and Donahue*, 2006] and associated parametric fits of these results [*Odum et al.*, 1996; *Hoffman et al.*, 1997; *Griffin et al.*, 1999] extrapolated to the relevant α- and β-pinene mixing ratios. If a simple linear regression is performed on the laboratory results for all oxidants (since the oxidant in the Appledore Island is probably a combination of multiple oxidants), the extrapolated line falls one to two orders of magnitude below the observed nanoparticle yields for aerosol mass production between 0.08 and 2 μg m^{-3}. Several models fall well below this linear fit since they assume a two-product model behavior. This result is consistent with the laboratory measurements,

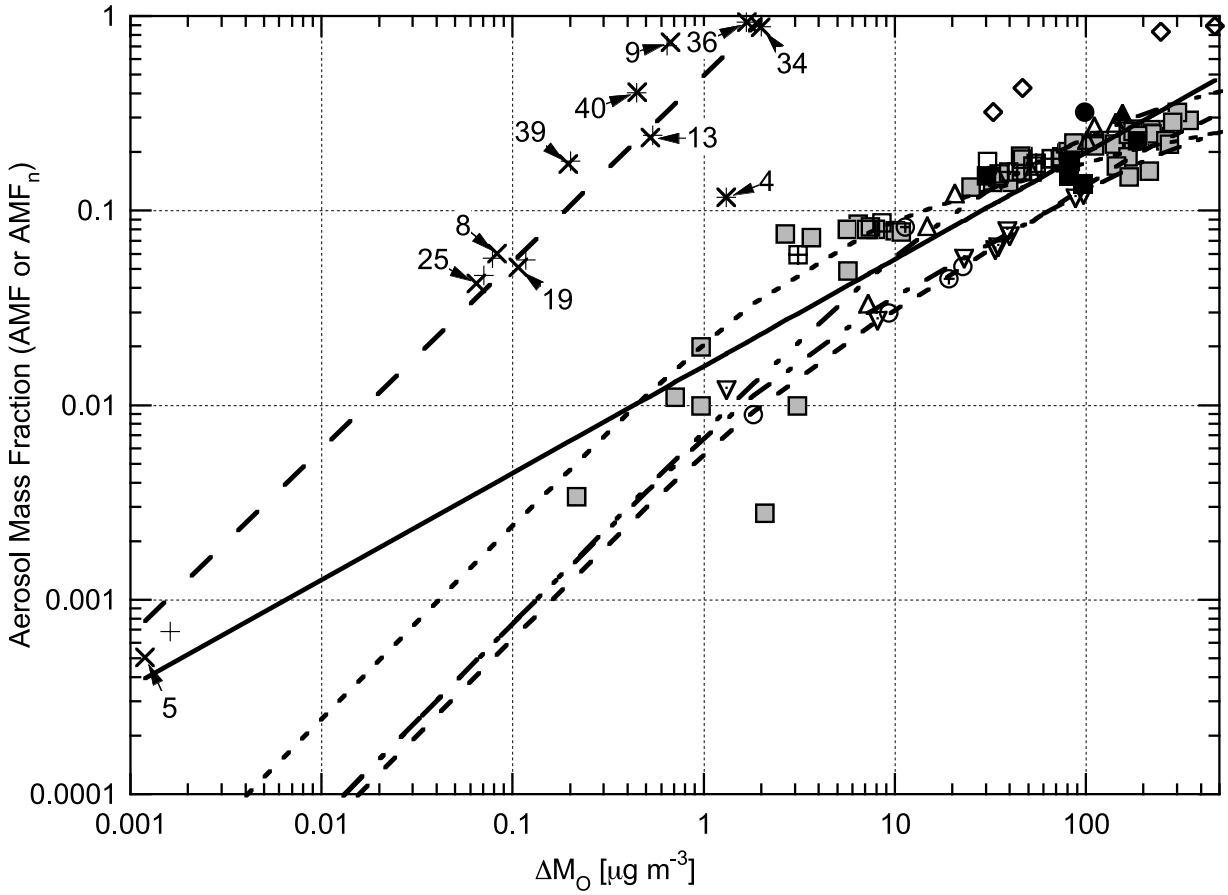

Figure 5. Measured particle AMF (yield) for laboratory studies of α-pinene oxidation products and apparent AMF_n (yield) for Appledore Island measurements of α- and β-pinene-correlated nanoparticle growth events. Apparent nanoparticle aerosol mass fractions (AMF_n) were calculated for observed changes in organic aerosol mass (ΔM_o) for each nanoparticle growth event on Appledore Island as the difference in the particle mass of the nanoparticle mode at the beginning and end of the event, using both the initial mode that was measured (pluses) and the initial mode calculated for a number-conserving growth event (crosses with event numbers). Laboratory measurements at temperatures ranging between 20°C and 40°C of yield (Y) versus change in organic aerosol mass (ΔM_o) are also shown for comparison. Symbols for these smog chamber experiments are shown for the type of experiment by shape with α-pinene + O_3 (squares), β-pinene + NO_3 (diamonds), β-pinene + O_3 (circles), β-pinene photo-oxidation (upward pointing triangles) and α-pinene photo-oxidation (downward pointing triangles) and by the experimental group by fill with *Griffin et al.* [1999] (unfilled), *Hoffmann et al.* [1997] (black fill), *Odum et al.* [1996] (center dot), *Hoppel et al.* [2001] (crosses), *Yu et al.* [1999] (center pluses), and *Presto and Donahue* [2006] (including references therein to *Presto et al.* [2005b] and *Cocker et al.* [2001]) (gray fill). The solid line is a linear regression to all of the laboratory measurements of yields summarized here. The dashed lines represent two parameter fits from the literature for α-pinene photo-oxidation [*Odum et al.*, 1996], β-pinene photo and ozone oxidation [*Griffin et al.*, 1999], and α-pinene ozone oxidation [*Hoffmann et al.*, 1997].

requiring only that those results not be extrapolated to lower values in order to model atmospheric conditions, and with *Odum et al.* [1996], since the premise of that model collapses when ΔM_0 is negligibly small.

5. Conclusions

[32] Observations at Appledore Island during ICARTT/CHAiOS 2004 of particle size distributions and ROG have shown that one third of all nanoparticle events and three fourths of all nanoparticle growth events were associated with peaks and subsequent losses of α- and β-pinene. These events occurred in the morning, consistent with photochemical driving forces for oxidant production and with regionally homogeneous air masses. The nanoparticles grew linearly, consistent with kinetic growth and a nearly constant source of condensable products for mass transfer. If α- and β-pinene are assumed to be the primary precursor, the yield or apparent AMF of SOA to the nanoparticle mode is significantly higher than is predicted by extrapolations of the two-product model to α- and β-pinene oxidation yields at low aerosol mass changes.

[33] Since it is difficult for laboratory experiments to mimic ambient α- and β-pinene concentrations well below 200 pptv and similarly low oxidant values, the estimated nanoparticle yields provide an appropriate yield for SOA in global models. These observations do not rule out the contributions of gas phase precursors other than α- and β-pinene; in fact, there is substantial evidence in at least 6 events that other factors were more important than α- and β-pinene. Isoprene may play a role in nanoparticle formation and growth, although the supermicron abundance of methane sulfonate is also consistent with isoprene contributing through particle phase reactions to formation of organosulfates [*Edney et al.*, 2005; *Kroll et al.*, 2005; *Jaoui et al.*, 2005; *Surratt et al.*, 2006; *Liggio and Li*, 2006; *Kleindienst et al.*, 2006; *Gao et al.*, 2006].

[34] Since the calculated apparent nanoparticle AMFs are significantly higher (by two orders of magnitude) than α- and β-pinene yields reported in controlled laboratory conditions, employing them in global models may simply act as a surrogate for other gas phase precursors which are as yet unidentified. The higher yields may be sufficient to account for the current discrepancy between modeled and observed organic particles [*Heald et al.*, 2005; *Chung and Seinfeld*, 2002; *Kanakidou et al.*, 2005]. Improving SOA parameterizations and resolving these discrepancies would have important implications for organic aerosol contributions to global radiative forcing.

[35] **Acknowledgments.** This work is a contribution to the ICARTT/CHAIOS program, supported by National Science Foundation grants ATM04-01611 and ATM04-01622. We also very much appreciate assistance in assembling and operating the instruments in the field operations from Susanne Marquardt, Roland von Glasow, Charlie Stanier, Spyros Pandis, Cynthia Randles, and Alice Delia. We are also grateful to Andreas Stohl for compiling the FLEXPART analyses, Robert Griffin for his comments on secondary organic aerosol formation, and two anonymous reviewers for their careful comments. Some gas phase pollutant and precursor data were obtained from the University of New Hampshire's AIRMAP Observing Stations, which are supported through the Office of Oceanic and Atmospheric Research at NOAA under grants NA05OAR4600154 and NA05OAR4601080. This paper is contribution 137 to the Shoals Marine Laboratory.

References

Aalto, P., et al. (2001), Physical characterization of aerosol particles during nucleation events, *Tellus, Ser. B*, *53*, 344–358.

Atkinson, R., and J. Arey (2003), Gas-phase tropospheric chemistry of biogenic volatile organic compounds: A review, *Atmos. Environ.*, *37*, S197–S219.

Bilde, M., and S. N. Pandis (2001), Evaporation rates and vapor pressures of individual aerosol species formed in the atmospheric oxidation of α- and β-pinene, *Environ. Sci. Technol.*, *35*, 3344–3349.

Birmili, W., A. Wiedensohler, C. Plass-Dulmer, and H. Berresheim (2000), Evolution of newly formed aerosol particles in the continental boundary layer: A case study including OH and H_2SO_4 measurements, *Geophys. Res. Lett.*, *27*, 2205–2208.

Birmili, W., H. Berresheim, C. Plass-Dulmer, T. Elste, S. Gilge, A. Wiedensohler, and U. Uhrner (2003), The Hohenpeissenberg aerosol formation experiment (HAFEX): A long-term study including size-resolved aerosol, H_2SO_4, OH, and monoterpenes measurements, *Atmos. Chem. Phys.*, *3*, 361–376.

Cai, X., and R. J. Griffin (2006), Secondary aerosol formation from the oxidation of biogenic hydrocarbons by chlorine atoms, *J. Geophys. Res.*, *111*, D14206, doi:10.1029/2005JD006857.

Chung, S. H., and J. H. Seinfeld (2002), Global distribution and climate forcing of carbonaceous aerosols, *J. Geophys. Res.*, *107*(D19), 4407, doi:10.1029/2001JD001397.

Cocker, D. R., S. L. Clegg, R. C. Flagan, and J. H. Seinfeld (2001), The effect of water on gas-particle partitioning of secondary organic aerosol. Part I: Alpha-pinene/ozone system, *Atmos. Environ.*, *35*, 6049–6072.

Dal Maso, M., M. Kulmala, K. E. J. Lehtinen, J. M. Mäkelä, P. Aalto, and C. D. O'Dowd (2002), Condensation and coagulation sinks and formation of nucleation mode particles in coastal and boreal forest boundary layers, *J. Geophys. Res.*, *107*(D19), 8097, doi:10.1029/2001JD001053.

de Gouw, J. A., et al. (2005), The budget of organic carbon in a polluted atmosphere: Results from the New England Air Quality Study in 2002, *J. Geophys. Res.*, *110*, D16305, doi:10.1029/2004JD005623.

Draxler, R. R., and G. D. Rolph (2005), HYSPLIT (Hybrid Single-Particle Lagrangian Integrated Trajectory) model access via NOAA ARL READY, Air Resour. Lab., NOAA, Silver Spring Md. (Available at http://www.arl.noaa.gov/ready/hysplit4.html)

Edney, E. O., T. E. Kleindienst, M. Jaoui, M. Lewandowski, J. H. Offenberg, W. Wang, and M. Claeys (2005), Formation of 2-methyl tetrols and 2-methylglyceric acid in secondary organic aerosol from laboratory irradiated isoprene/NO_x/SO_2/air mixtures and their detection in ambient $PM_{2.5}$ samples collected in the eastern United States, *Atmos. Environ.*, *39*, 5281–5289.

Fehsenfeld, F. C., et al. (2006), International Consortium for Atmospheric Research on Transport and Transformation (ICARTT): North America to Europe—Overview of the 2004 summer field study, *J. Geophys. Res.*, *111*, D23S01, doi:10.1029/2006JD007829.

Fischer, E., A. Pszenny, W. Keene, J. Maben, A. Smith, A. Stohl, and R. Talbot (2006), Nitric acid phase partitioning and cycling in the New England coastal atmosphere, *J. Geophys. Res.*, *111*, D23S09, doi:10.1029/2006JD007328.

Gao, S., J. D. Surratt, E. M. Knipping, E. S. Edgerton, M. Shahgholi, and J. H. Seinfeld (2006), Characterization of polar organic components in fine aerosols in the southeastern United States: Identity, origin, and evolution, *J. Geophys. Res.*, *111*, D14314, doi:10.1029/2005JD006601.

Griffin, R. J., D. R. Cocker, R. C. Flagan, and J. H. Seinfeld (1999), Organic aerosol formation from the oxidation of biogenic hydrocarbons, *J. Geophys. Res.*, *104*, 3555–3567.

Griffin, R. J., C. A. Johnson, R. W. Talbot, H. Mao, R. S. Russo, Y. Zhou, and B. C. Sive (2004), Quantification of ozone formation metrics at Thompson Farm during the New England Air Quality Study (NEAQS) 2002, *J. Geophys. Res.*, *109*, D24302, doi:10.1029/2004JD005344.

Hansel, A., A. Jordan, R. Holzinger, P. Prazeller, W. Vogel, and W. Lindinger (1995), Proton-transfer reaction mass-spectrometry—Online trace gas-analysis at the ppb level, *Int. J. Mass Spectrom.*, *150*, 609–619.

Hatakeyama, S., K. Izumi, T. Fukuyama, and H. Akimoto (1989), Reactions of ozone with α-pinene and β-pinene in air: Yields of gaseous and particulate products, *J. Geophys. Res.*, *94*, 13,013–13,024.

Heald, C. L., D. J. Jacob, R. J. Park, L. M. Russell, B. J. Huebert, J. H. Seinfeld, H. Liao, and R. J. Weber (2005), A large organic aerosol source in the free troposphere missing from current models, *Geophys. Res. Lett.*, *32*, L18809, doi:10.1029/2005GL023831.

Held, A., A. Nowak, W. Birmili, A. Wiedensohler, R. Forkel, and O. Klemm (2004), Observations of particle formation and growth in a mountainous forest region in central Europe, *J. Geophys. Res.*, *109*, D23204, doi:10.1029/2004JD005346.

Hoffmann, T., J. R. Odum, F. Bowman, D. Collins, D. Klockow, R. C. Flagan, and J. H. Seinfeld (1997), Formation of organic aerosols from the oxidation of biogenic hydrocarbons, *J. Atmos. Chem.*, *26*, 189–222.

Hoppel, W., et al. (2001), Particle formation and growth from ozonolysis of α-pinene, *J. Geophys. Res.*, *106*(D21), 27,603–27,618.

Janson, R., K. Rosman, A. Karlsson, and H. C. Hansson (2001), Biogenic emissions and gaseous precursors to forest aerosols, *Tellus, Ser. B*, *53*, 423–440.

Jaoui, M., T. E. Kleindienst, M. Lewandowski, J. H. Offenberg, and E. O. Edney (2005), Identification and quantification of aerosol polar oxygenated compounds bearing carboxylic or hydroxyl groups. 2. Organic tracer compounds from monoterpenes, *Environ. Sci. Technol.*, *39*, 5661–5673.

Jordan, C. E., R. W. Talbot, and B. D. Keim (2000), Water-soluble nitrogen at the New Hampshire sea coast: HNO_3, aerosols, precipitation, and fog, *J. Geophys. Res.*, *105*, 26,403–26,431.

Kalberer, M., et al. (2004), Identification of polymers as major components of atmospheric organic aerosols, *Science*, *303*, 1659–1662, doi:10.1126/science.1092185.

Kanakidou, M., K. Tsigaridis, F. J. Dentener, and P. J. Crutzen (2000), Human-activity-enhanced formation of organic aerosols by biogenic hydrocarbon oxidation, *J. Geophys. Res.*, *105*, 9243–9254.

Kanakidou, M., et al. (2005), Organic aerosol and global climate modeling: A review, *Atmos. Chem. Phys.*, *5*, 1053–1123.

Kavouras, I. G., N. Mihalopoulos, and E. G. Stephanou (1998), Formation of atmospheric particles from organic acids produced by forests, *Nature*, *395*, 683–686.

Kavouras, I. G., N. Mihalopoulos, and E. G. Stephanou (1999), Secondary organic aerosol formation vs primary organic aerosol emission: In situ evidence for the chemical coupling between monoterpenes acidic photo-

oxidation products and new particle formation over forests, *Environ. Sci. Technol.*, *33*, 1028–1037.

Keene, W. C., A. A. P. Pszenny, J. R. Maben, E. Stevenson, and A. Wall (2004), Closure evaluation of size-resolved aerosol pH in the New England coastal atmosphere during summer, *J. Geophys. Res.*, *109*, D23307, doi:10.1029/2004JD004801.

Keene, W. C., J. Stutz, A. A. P. Pszenny, J. R. Maben, E. Fischer, A. M. Smith, R. von Glasow, S. Pechtl, B. C. Sive, and R. K. Varner (2007), Inorganic chlorine and bromine in coastal New England air during summer, *J. Geophys. Res.*, doi:10.1029/2006JD007689, in press.

Kleindienst, T. E., E. O. Edney, M. Lewandowski, J. H. Offenberg, and M. Jaoui (2006), Secondary organic carbon and aerosol yields from the irradiation of isoprene and a-pinene in the presence of NO_x and SO_2, *Environ. Sci. Technol.*, *40*, 3807–3812.

Kroll, J. H., N. L. Ng, S. M. Murphy, R. C. Flagan, and J. H. Seinfeld (2005), Secondary organic aerosol formation from isoprene photooxidation under high-NO_x conditions, *Geophys. Res. Lett.*, *32*, L18808, doi:10.1029/2005GL023637.

Kulmala, M., M. Dal Maso, J. M. Mäkelä, L. Pirjola, M. Väkevä, P. Aalto, P. Miikkulainen, K. Hameri, and C. D. O'Dowd (2001), On the formation, growth and composition of nucleation mode particles, *Tellus, Ser. B*, *53*, 479–490.

Kulmala, M., H. Vehkamaki, T. Petajda, M. Dal Maso, A. Lauri, V. M. Kerminen, W. Birmili, and P. H. McMurry (2004), Formation and growth rates of ultrafine atmospheric particles: A review of observations, *J. Aerosol. Sci.*, *35*, 143–176.

Leaitch, W. R., J. W. Bottenheim, T. A. Biesenthal, S.-M. Li, P. S. K. Liu, K. Asalian, H. Dryfhout-Clark, and F. Hopper (1999), A case study of gas-to-particle conversion in an eastern Canadian forest, *J. Geophys. Res.*, *104*, 8095–8111.

Lee, A., A. H. Goldstein, J. H. Kroll, N. L. Ng, V. Varutbangkul, R. C. Flagan, and J. H. Seinfeld (2006), Gas-phase products and secondary aerosol yields from the photooxidation of 16 different terpenes, *J. Geophys. Res.*, *111*, D17305, doi:10.1029/2006JD007050.

Liggio, J., and S.-M. Li (2006), Organosulfate formation during the uptake of pinonaldehyde on acidic sulfate aerosols, *Geophys. Res. Lett.*, *33*, L13808, doi:10.1029/2006GL026079.

Lunden, M., D. Black, M. McKay, K. Revzan, A. Goldstein, and N. Brown (2006), Characteristics of fine particle growth events observed above a forested ecosystem in the Sierra Nevada Mountains in California, *Aerosol Sci. Technol.*, *40*, 373–388.

Lyubovtseva, Y. S., L. Sogacheva, M. Dal Maso, B. Bonn, P. Keronen, and M. Kulmala (2005), Seasonal variations of trace gases, meteorological parameters, and formation of aerosols in boreal forests, *Boreal Environ. Res.*, *10*, 493–510.

Mäkelä, J. M., P. Aalto, V. Jokinen, T. Pohja, A. Nissinen, S. Palmroth, T. Markkanen, K. Seitsonen, H. Lihavainen, and M. Kulmala (1997), Observations of ultrafine aerosol particle formation and growth in boreal forest, *Geophys. Res. Lett.*, *24*, 1219–1222.

Mäkelä, J. M., I. K. Koponen, P. Aalto, and M. Kulmala (2000a), One-year data of submicron size modes of tropospheric background aerosol in southern Finland, *J. Aerosol Sci.*, *31*, 595–611.

Mäkelä, J. M., M. Dal Maso, L. Pirjola, P. Keronen, L. Laakso, M. Kulmala, and A. Laaksonen (2000b), Characteristics of the atmospheric particle formation events observed at a boreal forest site in southern Finland, *Boreal Environ. Res.*, *5*, 299–313.

Mao, H., and R. W. Talbot (2004), O_3 and CO in New England: Temporal variations and relationships, *J. Geophys. Res.*, *109*, D21304, doi:10.1029/2004JD004913.

O'Dowd, C. D., et al. (2002), A dedicated study of New Particle Formation and Fate in the Coastal Environment (PARFORCE): Overview of objectives and achievements, *J. Geophys. Res.*, *107*(D19), 8108, doi:10.1029/2001JD000555.

Odum, J. R., T. Hoffmann, F. Bowman, D. Collins, R. C. Flagan, and J. H. Seinfeld (1996), Gas/particle partitioning and secondary organic aerosol yields, *Environ. Sci. Technol.*, *30*, 2580–2585.

Pikelnaya, O., S. C. Hurlock, S. Trick, and J. Stutz (2007), Intercomparison of multiaxis and long-path differential optical absorption spectroscopy measurements in the marine boundary layer, *J. Geophys. Res.*, doi:10.1029/2006JD007727, in press.

Presto, A. A., and N. M. Donahue (2006), Investigation of α-pinene + ozone secondary organic aerosol formation at low total aerosol mass, *Environ. Sci. Technol.*, *40*, 3536–3543.

Presto, A. A., K. E. H. Hartz, and N. M. Donahue (2005a), Secondary organic aerosol production from terpene ozonolysis. 1. Effect of UV radiation, *Environ. Sci. Technol.*, *39*, 7036–7045.

Presto, A. A., K. E. H. Hartz, and N. M. Donahue (2005b), Secondary organic aerosol production from terpene ozonolysis. 2. Effect of NO_x concentration, *Environ. Sci. Technol.*, *39*, 7046–7054.

Pszenny, A. A. P., J. Moldanová, W. C. Keene, R. Sander, J. R. Maben, M. Martinez, P. J. Crutzen, D. Perner, and R. G. Prinn (2004), Halogen cycling and aerosol pH in the Hawaiian marine boundary layer, *Atmos. Chem. Phys.*, *4*, 147–168. (Available at http://www.atmos-chem-phys.org/acp/4/147)

Pszenny, A. A. P., E. V. Fischer, R. S. Russo, B. C. Sive, and R. K. Varner (2007), Estimates of Cl atom concentrations and hydrocarbon kinetic reactivity in surface air at Appledore Island, Maine (USA), during International Consortium for Research on Transport and Transformation/Chemistry of Halogens at the Isles of Shoals, *J. Geophys. Res.*, doi:10.1029/2006JD007725, in press.

Russell, L. M., D. H. Lenschow, K. K. Laursen, P. B. Krummel, S. T. Siems, A. R. Bandy, D. C. Thornton, and T. S. Bates (1998), Bidirectional mixing in an ACE 1 marine boundary layer overlain by a second turbulent layer, *J. Geophys. Res.*, *103*, 16,411–16,432.

Seibert, P., and A. Frank (2004), Source-receptor matrix calculation with a Lagrangian particle dispersion model in backward mode, *Atmos. Chem. Phys.*, *4*, 51–63.

Seinfeld, J. H., and S. N. Pandis (1998), *Atmospheric Chemistry and Physics*, John Wiley, Hoboken, N. J.

Sive, B. C., Y. Zhou, D. Troop, Y. L. Wang, W. C. Little, O. W. Wingenter, R. S. Russo, R. K. Varner, and R. Talbot (2005), Development of a cryogen-free concentration system for measurements of volatile organic compounds, *Anal. Chem.*, *77*, 6989–6998.

Smith, A. M., W. C. Keene, J. R. Maben, A. A. P. Pszenny, and E. Fischer (2007), Ammonia sources, transport, transformation, and deposition in coastal New England during summer, *J. Geophys. Res.*, doi:10.1029/2006JD007574, in press.

Stanier, C. O., A. Y. Khlystov, and S. N. Pandis (2004), Nucleation events during the Pittsburgh air quality study: Description and relation to key meteorological, gas phase, and aerosol parameters, *Aerosol Sci. Technol.*, *38*, 253–264.

Stohl, A., C. Forster, S. Eckhardt, N. Spichtinger, H. Huntrieser, J. Heland, H. Schlager, S. Wilhelm, F. Arnold, and O. Cooper (2003), A backward modeling study of intercontinental pollution transport using aircraft measurements, *J. Geophys. Res.*, *108*(D12), 4370, doi:10.1029/2002JD002862.

Stohl, A., C. Forster, A. Frank, P. Seibert, and G. Wotawa (2005), Technical note: The Lagrangian particle dispersion model FLEXPART version 6.2, *Atmos. Chem. Phys.*, *5*, 2461–2474.

Surratt, J. D., et al. (2006), Chemical composition of secondary organic aerosol formed from the photooxidation of isoprene, *J. Phys. Chem. A*, *110*, 9665–9690.

Talbot, R., H. Mao, and B. Sive (2005), Diurnal characteristics of surface level O_3 and other important trace gases in New England, *J. Geophys. Res.*, *110*, D09307, doi:10.1029/2004JD005449.

Wehner, B., T. Petaja, M. Boy, C. Engler, W. Birmili, T. Tuch, A. Wiedensohler, and M. Kulmala (2005), The contribution of sulfuric acid and non-volatile compounds on the growth of freshly formed atmospheric aerosols, *Geophys. Res. Lett.*, *32*, L17810, doi:10.1029/2005GL023827.

Yu, J. Z., D. R. Cocker, R. J. Griffin, R. C. Flagan, and J. H. Seinfeld (1999), Gas-phase ozone oxidation of monoterpenes: Gaseous and particulate products, *J. Atmos. Chem.*, *34*, 207–258.

Zhang, R. Y., I. Suh, J. Zhao, D. Zhang, E. C. Fortner, X. X. Tie, L. T. Molina, and M. J. Molina (2004), Atmospheric new particle formation enhanced by organic acids, *Science*, *304*, 1487–1490.

Zhou, Y., R. K. Varner, R. S. Russo, O. W. Wingenter, K. B. Haase, R. Talbot, and B. C. Sive (2005), Coastal water source of short-lived halocarbons in New England, *J. Geophys. Res.*, *110*, D21302, doi:10.1029/2004JD005603.

E. V. Fischer, Department of Atmospheric Sciences, University of Washington, Seattle, WA 98195, USA.

W. C. Keene, Department of Environmental Science, University of Virginia, Charlottesville, VA 22904, USA.

A. A. Mensah and L. M. Russell, Scripps Institution of Oceanography, University of California, San Diego, La Jolla, CA 92093, USA. (lmrussell@ucsd.edu)

A. A. P. Pszenny, Mount Washington Observatory, University of New Hampshire, Durham, NH 03860, USA.

B. C. Sive and R. K. Varner, Climate Change Research Center, Institute for the Study of Earth, Oceans, and Space, University of New Hampshire, Durham, NH 03824, USA.

J. Stutz, Department of Atmospheric and Ocean Sciences, University of California, Los Angeles, CA 90095, USA.